Superlattices and Microstructures 47 (2010) 550–555

Contents lists available at ScienceDirect

Superlattices and Microstructures

journal homepage: www.elsevier.com/locate/superlattices

Inelastic phonon interactions at solid–graphite interfaces

John C. Duda [a,*], Patrick E. Hopkins [b,1], Thomas E. Beechem [b], Justin L. Smoyer [a], Pamela M. Norris [a,2]

[a] Department of Mechanical and Aerospace Engineering, University of Virginia, Charlottesville, VA 22904, United States
[b] Engineering Sciences Center, Sandia National Laboratories, Albuquerque, NM 87185, United States

ARTICLE INFO

Article history:
Received 26 October 2009
Accepted 8 January 2010
Available online 20 January 2010

Keywords:
Inelastic
Graphite
Thermal boundary conductance
Phonon
Transport
Interface

ABSTRACT

The presented model predicts thermal boundary conductance at interfaces where one material comprising the junction is characterized by high elastic anisotropy. In contrast to previous approaches, the current methodology accounts for contributions from inelastic scattering through consideration of multiple-phonon interactions. Inelastic contributions become significant as the temperature, as well as the degree of acoustic mismatch between the materials, increases. Inclusion of the inelastic interactions is necessary for a variety of interfacial systems including the metal–graphite boundary examined here. Improvement is shown over existing approaches that address only elastic scattering as both three- and four-phonon interactions significantly augment the transport.

Allotropes of carbon, specifically carbon nanotubes (CNTs) and graphite, continue to be integrated into existing thermal abatement solutions. CNT-based thermal interface materials (TIMs) [1,2] and graphite-reinforced metal heat spreaders [3,4] both serve as examples of how the unique thermal and mechanical properties of sp^2-type carbon structures can greatly enhance existing technologies. Still, the overall performance of any carbon-enhanced thermal abatement solution can be limited due to the interface between the tightly bonded sp^2 carbon atoms and the contacting material, which, in many applications, is a metal. It is likely that the thermal boundary conductance (h_{BD}) at metal–graphite or metal–CNT interfaces is low due to a combination of reduced dimensionality and anisotropy of the carbon-based materials, as well as the large acoustic mismatch between the materials [5,6]. The ability

* Corresponding author. Tel.: +1 434 982 2736; fax: +1 434 982 2037.
E-mail addresses: duda@virginia.edu (J.C. Duda), pehopki@sandia.gov (P.E. Hopkins), pamela@virginia.edu (P.M. Norris).
1 Tel.: +1 505 284 5729.
2 Tel.: +1 434 924 6295.

0749-6036/$ – see front matter © 2010 Elsevier Ltd. All rights reserved.
doi:10.1016/j.spmi.2010.01.001

to accurately predict h_{BD} at metal–carbon interfaces is important for the optimization of these hybrid material systems in thermal applications.

Predictive models do exist for thermal transport at metal–CNT [7] and metal–graphite interfaces [8], but they consider only elastic phonon scattering events at the interface, as they are based on the the diffuse mismatch model (DMM) [9]. The role of inelastic scattering during diffusive interfacial transport processes at interfaces characterized by large acoustic mismatch has been demonstrated both experimentally [5,10] and through the use of classical molecular dynamics [11]. It is reasonable to assume that inelastic scattering events contribute significantly during transport processes at metal–CNT and metal–graphite interfaces due to the large acoustic mismatch between these materials (the maximum phonon frequencies of graphite [12] are several times that of most metals).

Recently, a model has been presented to directly consider multiple-phonon processes contributing to inelastic scattering at solid–solid interfaces [13]. Through conservation of energy and phonon population, this model allows for the decay of high-energy phonons at frequency $n\omega$ into n lower-energy phonons each at frequency ω, where n is an integer. However, this model assumes that isotropic materials comprise both sides of the interface. At the interface between metal and graphite or CNTs, this is clearly not the case. The model presented here accounts for inelastic scattering at interfaces where one material comprising the interface is characterized by high elastic anisotropy. The metal–graphite interface will be considered during the development of this model, but this approach can be easily extended to other anisotropic materials.

The extreme anisotropy of graphite is evident when examining the thermal conductivity, where the a-axis (in the basal plane) and c-axis (perpendicular to the basal plane) values differ by three to four orders of magnitude [14,15]. As a result of this anisotropy, the phonon dispersion relationships for graphite are quite complicated. However, at temperatures above cryogenic, the strong anisotropy of graphite allows for certain simplifying assumptions. The interaction between individual monolayers in the graphite structure can be described as a van der Waals type interaction, which is associated with low-frequency vibrations. Dispersion diagrams of graphite show that acoustic interlayer vibrations exist at frequencies below 3 THz, one to two orders of magnitude below the longitudinal and transverse cutoff frequencies within the basal plane [12]. Additionally, studies examining both CNTs and graphite have indicated that interlayer acoustic modes saturate at temperatures above 50 K [7,16].

As a result of this weak interlayer vibrational coupling, an effective Debye density of states can be used to describe bulk graphite at temperatures above cryogenic [8,15]. The formulation of an effective density of states rests on describing graphite by its basal- or cross-plane attributes, depending on the property of concern. Developing the effective density of states for predictions of h_{BD}, one can consider first a single monolayer of graphite, described by a two-dimensional Debye density of states. Scaling this density of states by N, or the number of two-dimensional subsystems per unit length, generates an effective density of states for the graphite system. The density of states for bulk graphite thus becomes

$$D_{\text{eff}}(\omega, v_{a,j}) = N\frac{\omega}{2\pi v_{a,j}^2} = \frac{\omega}{2\pi v_{a,j}^2}\frac{1}{d}, \tag{1}$$

where d is the interlayer spacing and $v_{a,j}$ is the polarization-specific Debye phonon group velocity in the basal plane. Therefore, the thermal flux in graphite perpendicular to the interface is given by

$$q_{g,j,z} = \pi \sum_j \int_{\omega_{a,j}} \hbar\omega v_{z,j} D_{\text{eff}}(\omega, v_{a,j}) f \,\mathrm{d}\omega, \tag{2}$$

here $\hbar$ is Planck's constant divided by 2π, ω is the phonon angular frequency, and f is the Bose–Einstein distribution function. The subscript z denotes the orientation of the graphite relative to the interface and can take on two values, either a (basal planes perpendicular to the interface, transport along the basal planes), or c (basal planes parallel to the interface, transport perpendicular to the planes). Note that the density of states and cutoff frequency do not depend on the graphite orientation since the vibrational modes are assumed only to exist in the basal plane. Still, the propagation velocity does depend on the orientation. Three modes of vibration are still assumed within graphite (one longitudinal, two degenerate transverse) for either orientation and are taken as $v_{a,l} = 23{,}600$ m/s,

Table 1
Individual contributions of two-, three-, and four-phonon processes, as well as the total predicted and experimental values [19] for metal-to-*c*-axis h_{BD} at 300 K. The inclusion of three- and four-phonon processes increases the accuracy of the model. Experimental data for the Au–graphite interface is not available at this time, but the predicted values are included to illustrate the relative contribution of each process as the acoustic mismatch between metal and graphite increases.

	2-phonon (MW/m^2 K)	3-phonon (MW/m^2 K)	4-phonon (MW/m^2 K)	Total predicted (MW/m^2 K)	Experimental (MW/m^2 K)
Al	30.5	8.5	2.0	41.0	50
Au	9.1	4.0	1.6	14.7	n/a

$\nu_{a,t} = 15{,}900$ m/s, $\nu_{c,l} = 1{,}960$ m/s, and $\nu_{c,t} = 700$ m/s [15]. Assuming a planar lattice point density in graphite as $N_a = 1.9 \times 10^{19}$ m^{-2}, the *a*-axis cutoff frequency is defined as $\omega_{a,j} = \nu_{a,j}\sqrt{4\pi N_a}$. The thermal boundary conductance from a metal film to a graphite substrate is then given by

$$h_{BD}^{1\to g,z} = \frac{1}{4}\sum_{j}^{3}\int_{\omega_{D,j}} \hbar\,\omega\,\nu_{1,j}\,D_1(\omega,\nu_{1,j})\,\frac{\partial f}{\partial T}\,\zeta^{1\to g,z}(\omega)\;\mathrm{d}\omega, \tag{3}$$

where the metal properties are denoted by the subscript or superscript "1". In this work, a three-dimensional isotropic Debye density of states is used to describe the metal film, and $\omega_{D,j} = \nu_{1,j}\sqrt[3]{6\pi^2 N_a}$ [17]. Values for the density, ρ_1, and velocities, $\nu_{1,j}$ are taken from Swartz and Pohl [9]. The transmission coefficient from the metal film to the graphite substrate, $\zeta^{1\to g,z}$, is taken as frequency dependent since this work considers two-, three-, and four-phonon processes, discussed below.

Following the theory from previous work developed to account for multiple-phonon diffusive scattering events at solid–solid interfaces [13], the thermal boundary conductance in Eq. (3) is redefined to explicitly describe two- (elastic), three-, and four-phonon (both inelastic) processes, yielding

$$h_{BD}^{1\to g,z} = \frac{1}{4}\sum_{j}^{3}\int_{\omega_{D,j}} \hbar\,\omega\,\nu_{1,j}\,D_1(\omega,\nu_{1,j})\,\frac{\partial f}{\partial T}\left(\zeta_{(2),j}^{1\to g,z}(\omega)+\zeta_{(3)}^{1\to g,z}(\omega)+\zeta_{(4)}^{1\to g,z}(\omega)\right)\mathrm{d}\omega, \tag{4}$$

where the transmission coefficient is separated into its two-, three-, and four-phonon components. Here, the two-phonon elastic transmission coefficient is defined as outlined in the original development of the DMM [9] so that detailed balance on each phonon frequency assuming two-phonon scattering yields

$$\hbar\omega D_1(\omega,\nu_{1,j})f(\omega)\zeta_{(2),j}^{1\to g,z}(\omega) = \hbar\omega D_{\mathrm{eff}}(\omega,\nu_{a,j})f(\omega)\zeta_{(2),j}^{g,z\to 1}(\omega), \tag{5}$$

which, assuming completely diffusive scattering ($\zeta^{1\to g,z} = 1-\zeta^{g,z\to 1}$), yields a two-phonon transmission coefficient of

$$\zeta_{(2),j}^{1\to g,z} = \frac{\frac{\nu_{z,j}}{\nu_{a,j}^2}\frac{1}{d}}{\frac{\omega}{\pi\nu_{1,j}^2}+\frac{\nu_{z,j}}{\nu_{a,j}^2}\frac{1}{d}}. \tag{6}$$

The frequency dependence of the phonon distribution, f, has been included for clarity in the development of the higher-order phonon processes. Note that, in the development of Eq. (6), the transmission coefficient is calculated on a per frequency, as well as per polarization, basis. Such an approach assumes not only completely elastic processes but also, in contrast to typical approaches of diffuse scattering, that a phonon of mode *j* can only couple with another phonon of the same mode. This development is necessary, however, in order to insure phonon number conservation for both the elastic and the higher-order processes [13]. Although this abandons the pure definition of diffuse scattering (the phonon loses memory and can scatter to any mode), in the Debye approximation, this assumption does not make a substantial difference in the overall result [18]. To calculate the the three-phonon transmission probability, we perform a similar balance shown in Eq. (5) only assuming

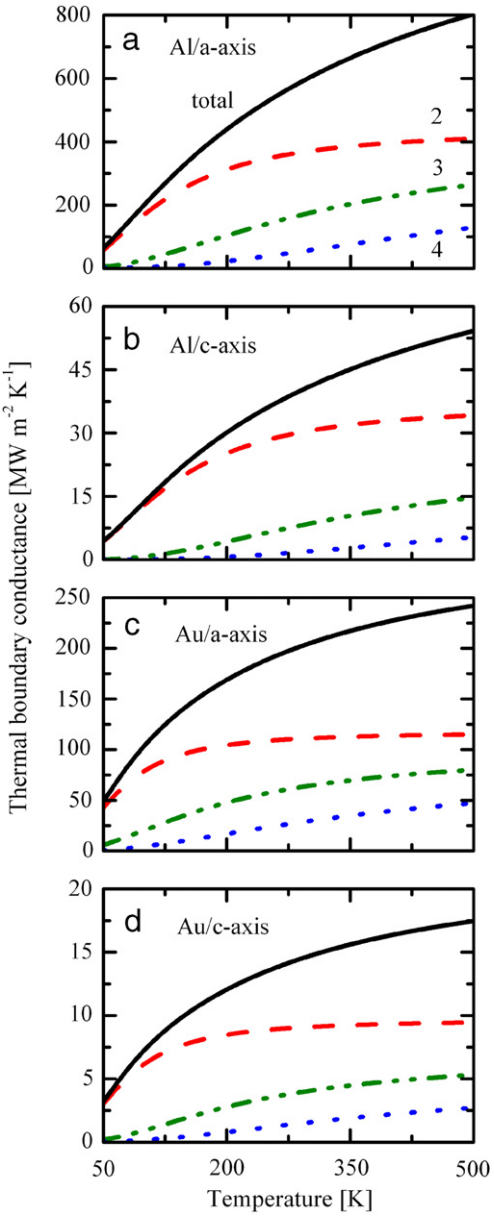

Fig. 1. Temperature-dependent h_{BD} at Al–graphite and Au–graphite interfaces for both orientations of graphite, as well as the individual contributions from two-, three-, and four-phonon processes. Higher-order inelastic phonon processes become more significant to the overall value of h_{BD} with increased temperature, as well as increased acoustic mismatch (the Au–graphite mismatch is greater than that of Al–graphite).

that two phonons of energy ω in the metal will couple with a phonon of energy 2ω in the substrate, so that the balance equation becomes

$$2\hbar\omega\nu_{1,j}D_1(\omega, \nu_{1,j})f(\omega)\zeta_{(3),j}^{1\to g,z}(1-\zeta_{(2),j}^{1\to g,z}) = \hbar(2\omega)\nu_{z,j}D_{\text{eff}}(2\omega, \nu_{a,j})f(2\omega)(1-\zeta_{(3),j}^{1\to g,z})\zeta_{(2),j}^{1\to g,z}, \quad (7)$$

when $0 < \omega \leq \frac{1}{2}\omega_{\mathrm{D},j}$ and

$$2\hbar\omega\nu_{1,j}D_1(\omega, \nu_{1,j})f(\omega)\zeta_{(3),j}^{1\to g,z}(1-\zeta_{(2),j}^{1\to g,z}) = \hbar(2\omega)\nu_{z,j}D_{\mathrm{eff}}(2\omega, \nu_{a,j})f(2\omega)\zeta_{(3),j}^{g,z\to 1}, \tag{8}$$

when $\frac{1}{2}\omega_{\mathrm{D},j} < \omega \leq \omega_{\mathrm{D},j}$, where $f(2\omega) = [\exp(\hbar(2\omega)/k_{\mathrm{B}}T) - 1]^{-1}$. This gives a three-phonon transmission coefficient, defined as

$$\zeta_{(3),j}^{1\to g,z} = \begin{cases} \dfrac{\frac{\nu_{z,j}}{\nu_{a,j}^2}\frac{1}{d}f(2\omega)\zeta_{(2),j}^{1\to g,z}}{\frac{\omega}{2\pi\nu_{a,j}^2}f(\omega)(1-\zeta_{(2),j}^{1\to g,z}) + \frac{\nu_{z,j}}{\nu_{a,j}^2}\frac{1}{d}f(2\omega)\zeta_{(2),j}^{1\to g,z}}, & 0 < \omega \leq \dfrac{1}{2}\omega_{\mathrm{D},j} \\ \dfrac{\frac{\nu_{z,j}}{\nu_{a,j}^2}\frac{1}{d}f(2\omega)}{\frac{\omega}{2\pi\nu_{a,j}^2}f(\omega)(1-\zeta_{(2),j}^{1\to g,z}) + \frac{\nu_{z,j}}{\nu_{a,j}^2}\frac{1}{d}f(2\omega)}, & \dfrac{1}{2}\omega_{\mathrm{D},j} < \omega \leq \omega_{\mathrm{D},j}. \end{cases} \tag{9}$$

The development of the four-phonon process follows in a similar fashion, but has been omitted from this work for the sake of brevity. In general, for an n-phonon process, there will be $n-1$ frequency intervals when calculating $\zeta_{(n),j}^{1\to g,z}$ [13]. In this work, the discussion is limited to four and fewer phonon processes, as the contributions of higher-order processes do not significantly contribute to h_{BD} at lower temperatures [13]. While this treatment of inelastic scattering may not be exact, it serves as a good first approximation to the relative contribution of inelastic processes to thermal transport at interfaces.

Predicted temperature-dependent h_{BD} at Al–graphite and Au–graphite interfaces for both orientations of graphite, as well as the individual contributions from two-, three-, and four-phonon processes, are shown in Fig. 1. By examining the plots, it is apparent that considerations of inelastic processes are more important as the acoustic mismatch and temperature increase (Au has a lower Debye temperature than Al, 165 K and 428 K, respectively [17], and is therefore more acoustically mismatched with graphite). Table 1 lists the contributions of each process, as well as the total predicted and experimental values [19] for metal-to-c-axis h_{BD} at 300 K. In general, it is apparent that this model, in which inelastic processes are considered, agrees better with the experimental data than the two-phonon process alone [8], reducing the underprediction from 39% (elastic only) to 18% (up to four-phonon inelastic).

In summary, a model has been derived to account for multiple-phonon inelastic scattering processes in predictions of h_{BD} at the interfaces between isotropic and anisotropic materials. Example calculations are performed for Al–graphite and Au–graphite interfaces. Improved agreement between the model and experimental data has been shown for the Al–graphite interface. The higher-order phonon processes show an increasing contribution to the overall h_{BD} as the materials comprising the interface become increasingly vibrationally dissimilar.

Acknowledgements

J.C.D., J.L.S., and P.M.N. acknowledge the financial support of the Office of Naval Research through a MURI grant (Grant No. N00014-07-1-0723) and the financial support of the Air Force Office of Scientific Research (Grant No. FA9550-09-1-0245). J.C.D. is greatly appreciative of financial support from the National Science Foundation through the Graduate Research Fellowship Program. P.E.H. is grateful for funding from the LDRD program office through the Sandia National Laboratories Harry S. Truman Fellowship. Sandia is a multiprogram laboratory operated by Sandia Corporation, a Lockheed-Martin Company, for the United States Department of Energy's National Nuclear Security Administration under Contract DE-AC04-94AL85000.

References

[1] J. Xu, T.S. Fisher, Enhancement of thermal interface materials with carbon nanotube arrays, Int. J. Heat Mass Transfer 49 (2009) 1658–1666.
[2] T. Tong, Y. Zhao, L Delzeit, A. Kashani, M. Meyyappan, A. Majumdar, Dense vertically aligned multiwalled carbon nanotube arrays as thermal interface materials, IEEE Trans. Comp. Pack. Technol. 20 (2007) 92–100.

[3] P.B. Abel, A.L. Korenyi-Both, F.S. Honecy, S.V. Pepper, Study of copper on graphite with titanium or chromium bond layer, J. Mater. Res. 9 (1994) 617–624.
[4] K. Datta, S.N. Tewari, J.E. Gatica, W. Shih, L. Bentsen, Copper-alloy impregnated carbon–carbon hybrid composites for electronic packaging applications, Metal. Mater. Trans. A 30A (2009) 175–181.
[5] H.-K. Lyeo, D.G. Cahill, Thermal conductance of interfaces between highly dissimilar materials, Phys. Rev. B 73 (2006) 144301.
[6] R.J. Stevens, A.N. Smith, P.M. Norris, Measurement of thermal boundary conductance of a series of metal-dielectric interfaces by the transient thermoreflectance technique, J. Heat Transfer 127 (2005) 315–322.
[7] R. Prasher, Thermal boundary resistance and thermal conductivity of multiwalled carbon nanotubes, Phys. Rev. B 77 (2008) 075424.
[8] J.C. Duda, J.L. Smoyer, P.M. Norris, P.E. Hopkins, Extension of the diffuse mismatch model for thermal boundary conductance between isotropic and anisotropic materials, Appl. Phys. Lett. 95 (2009) 031912.
[9] E.T. Swartz, R.O. Pohl, Thermal boundary resistance, Rev. Modern Phys. 61 (1989) 605–667.
[10] P.E. Hopkins, P.M. Norris, R.J. Stevens, Influence of inelastic scattering at metal-dielectric interfaces, J. Heat Transfer 130 (2008) 022401.
[11] R.J. Stevens, L.V. Zhigilei, P.M. Norris, Effects of temperature and disorder on thermal boundary conductance at solid–solid interfaces: nonequilibrium molecular dynamics simulations, Int. J. Heat Mass Transfer 50 (2007) 3977–3989.
[12] R. Nicklow, N. Wakabayashi, H.G. Smith, Lattice dynamics of pyrolytic graphite, Phys. Rev. B 5 (1972) 4951–4962. 1972.
[13] P.E. Hopkins, Multiple phonon processes contributing to inelastic scattering during thermal boundary conductance at solid interfaces, J. Appl. Phys. 106 (2009) 013528.
[14] F.P. Incropera, D.P. DeWitt, Fundamentals of Heat and Mass Transfer, Wiley, Hoboken, NJ, 2002.
[15] K. Sun, M.A. Stroscio, M. Dutta, Graphite c-axis thermal conductivity, Superlattices Microstruct. 45 (2009) 60–64.
[16] P. Kim, L. Shi, A. Majumdar, P.L. McEuen, Thermal transport measurements of individual multiwalled nanotubes, Phys. Rev. Lett. 87 (2001) 215502.
[17] C. Kittel, Introduction to Solid State Physics, Wiley, Hoboken, NJ, 2005.
[18] J.C. Duda, J.L. Smoyer, P.M. Norris, P.E. Hopkins, On the assumption of detailed balance in prediction of diffusive transmission probability during interfacial transport. Nano. Micro. Thermophys. Eng. (in press).
[19] A.J. Schmidt, X. Chen, G. Chen, Pulse accumulation, radial heat conduction, and anisotropic thermal conductivity in pump-probe transient thermoreflectance, Rev. Sci. Instrum. 79 (2008) 114902.